Phase transition and critical behavior of spin–orbital coupled spinel ZnV_2O_4*

Li Wang(王理)[1], Rong-juan Wang(王蓉娟)[1], Yuan-yuan Zhu(朱媛媛)[2], Zhi-hong Lu(卢志红)[3], Rui Xiong(熊锐)[1], Yong Liu(刘雍)[1,†], and Jing Shi(石兢)[1,‡]

[1] *Key Laboratory of Artificial Micro- and Nano-structures of Ministry of Education and School of Physics and Technology, Wuhan University, Wuhan* 430072, *China*

[2] *High Magnetic Field Laboratory, Chinese Academy of Sciences, Hefei* 230031, *China*

[3] *School of Materials and Metallurgy, Wuhan University of Science and Technology, Wuhan* 430081, *China*

(Received 5 August 2015; revised manuscript received 9 September 2015; published online 30 November 2015)

We present the temperature-dependent susceptibility and specific heat measurement of spinel ZnV_2O_4. The structural transition with orbital ordering and the antiferromagnetic transition with spin ordering were observed at 50 K and 37 K, respectively. By analysis of the hysteresis behavior between the specific heat curves obtained in warming and cooling processes, the structural transition was confirmed to be the first-order transition, while the antiferromagnetic transition was found to be of the second-order type. At the structural transition, the latent heat and entropy change were calculated from the excess specific heat, and the derivative of pressure with respect to temperature was obtained using the Clausius–Clapayron equation. At the magnetic transition, the width of the critical fluctuation region was obtained to be about 0.5 K by comparing with Gaussian fluctuations. In the critical region, the critical behavior was analyzed by using renormalization-group theory. The critical amplitude ratio $A^+/A^- = 1.46$, which deviates from the 3D Heisenburg model; while the critical exponent α is -0.011, which is close to the 3D XY model. We proposed that these abnormal critical behaviors can be attributed to strong spin–orbital coupling accompanied with the antiferromagnetic transition. Moreover, in the low temperature range (2–5 K), the Fermi energy, the density of states near the Fermi surface, and the low limit of Debye temperature were estimated to be 2.42 eV, 2.48 eV^{-1}, and 240 K, respectively.

Keywords: spinel compounds, specific heat, phase transition, critical behavior

PACS: 68.35.Rh, 75.40.–s, 64.60.–I, 82.60.Fa **DOI:** 10.1088/1674-1056/25/1/016802

1. Introduction

The $S = 1$ spinel compound ZnV_2O_4 has attracted much interest in recent years due to its novel applications in the energy area such as hydrogen storage,[1–4] as well as the unique physical properties of 3d electrons arising from strong coupling among charge, spin, orbit, and lattice.[5] At room temperature, the V^{3+} ions form a corner-sharing, geometrically frustrated, pyrochlore network and are octahedrally coordinated by six oxygen ions, while the Zn^{2+} ions are located in four tetrahedral oxygen ions, presenting the cubic symmetry $Fd\bar{3}M$.[6] With temperature dropping, the symmetry of the lattice is broken by a structural transition induced by the Jahn–Teller effect.[6] Such transition leading by a lattice distortion was originally observed by Ueda's team via peak splitting in the x-ray diffraction (XRD) pattern around the transition temperature $T_S = 50$ K.[7] They found that ZnV_2O_4 is cubic above 50 K while tetragonal below 48 K with a compression along the c axis ($c/a \approx 0.994$).[7] Accompanied by this structural transition, a kind of orbital ordering emerges at the same temperature on account of the split of the t_{2g} level and the reoccupation of two lower energy levels by two electrons of V^{3+}.[8] Tsunetsugu and Motome believed that the Coulomb and exchange interaction between V^{3+}'s played a decisive role, thus one electron of each V^{3+} invariably occupied d_{xy} and another one occupied d_{zx} and d_{yz} alternatively.[9,10] However, based on the relativistic spin–orbit coupling effect, Tchernyshyov proposed a ferro-type orbital order with complex orbital state $d_{xz} \pm i d_{yz}$ consistent with the system symmetry $I4_1/amd$.[11] On the other hand, neutron scattering experiments and the susceptibility result witnessed that a Néel transition from paramagnetism (PM) to antiferromagnetism (AFM) at transition temperature $T_M = 40$ K exists in ZnV_2O_4 as well.[7,12,13] The configuration of such antiferromagnetic spin chains is still ambiguous owing to the geometric frustration and the spin–orbital coupling. Those two transitions were obviously observed in temperature-dependent susceptibility and specific heat by Vasiliev *et al.*[14] Although the two transition temperatures obtained by them, 45 K and 31 K, are lower than those identified in XRD and neutron scattering experiments, Vasiliev's work[14] revealed that the structural and orbital tran-

*Project supported by the National Basic Research Program of China (Grant No. 2012CB821404), the National Natural Science Foundation of China (Grant Nos. 51172166 and 61106005), the National Science Fund for Talent Training in Basic Science, China (Grant No. J1210061), and the Doctoral Fund of Ministry of Education of China (Grant No. 20110141110007).

†Corresponding author. E-mail: yongliu@whu.edu.cn

‡Corresponding author. E-mail: jshi@whu.edu.cn

© 2016 Chinese Physical Society and IOP Publishing Ltd

sition is a first-order transition, while the AFM transition is a second-order one.

As is well known, the second-order transition is a continuous transition, whose critical behaviors and universal classifications could provide a deep insight into such transition, as well as the inherent relations between the transition and various interactions.[15] Thus, a lot of investigations of critical behaviors have been carried out for the second-order phase transitions with ferromagnetic and antiferromagnetic orders, as well as superconductive orders. However, few investigations into the critical behaviors of ferromagnetic or antiferromagnetic transition with the coexistence of spin–spin interaction and spin–orbital couplings were reported, especially in AB_2X_4 spinel compounds. The critical behaviors of paramagnetic–ferrimagnetic and paramagnetic–ferromagnetic transitions with the competitions between spin, orbital, and lattice degrees of freedom were studied in MnV_2O_4 and $CdCr_2S_4$ by Zhang's group and Lou's group, respectively.[16,17] They both observed the discrepancy of critical exponents with respect to either the Heisenberg model or the mean field theory, and revealed some possible effects of spin–orbital and spin–phonon couplings on the critical phenomena.[17] Different from MnV_2O_4 and $CdCr_2S_4$, the second-order phase transition in ZnV_2O_4 is a paramagnetic–antiferromagnetic transition. Moreover, for MnV_2O_4, the temperature of structural transition accompanied by the orbital ordering (T_S) is lower than the magnetic transition temperature T_M,[16] while for ZnV_2O_4, T_S is higher than T_M. This indicates that the AFM transition in ZnV_2O_4 is in the background of the orbital order. Obviously, it is significant to check the critical behavior of this kind of AFM transition accompanied with orbital order.

In this paper, the phase transitions and the critical behaviors of ZnV_2O_4 are investigated via susceptibility and specific heat measurements. The critical exponent and the critical fluctuation region accompanying the second-order AFM transition are obtained. An inconsistency of universal classification identified by either the critical exponent or the critical amplitude ratio is found in this compound. Moreover, the derivative of pressure with respect to temperature around the first-order structural transition is derived from the Clausius–Clapayron equation.

2. Experiments

The polycrystalline sample of ZnV_2O_4 was synthesized by solid-phase reaction using high purity powders of ZnO (Sinopharm, 99.99%) and V_2O_5 (Sinopharm, 99%). The starting powders were first mixed thoroughly at stoichiometric ratio; then the mixed powder was pressed into pellets and annealed at 800 °C for 24 h under H_2/N_2 (concentration of H_2 was 5%) mixed gas atmosphere. The obtained sample was a black bulk ceramic.

The crystal structure and phase purity of the sample were investigated by XRD by using Cu-$K\alpha$ radiation (D8 Advanced, Bruker AXS, Germany) with 2θ changing from 20° to 80° at room temperature. The temperature-dependent susceptibility and specific heat measurements were carried out on a physical properties measurement system (PPMS 6000, Quantum Design, USA). Specifically, the susceptibility against temperature (χ–T) was measured in a warming process from 2 K to 300 K under an applied field of 1 T after zero field cooling. The temperature-dependent specific heat (C_P–T) was measured between 2 K to 200 K in both cooling and warming processes without field. The data of specific heat were collected every 0.1 K in ranges of 2 K to 10 K and 30 K to 60 K, and every 0.01 K in the AFM transition region with a temperature range from 36 K to 39 K.

3. Results and discussion

The structure of the ZnV_2O_4 sample is characterized by XRD at room temperature. The XRD pattern is shown in Fig. 1; all characteristic peaks perfectly match the standard data without any redundant peak.[18] The obtained average lattice constant of our sample is 8.399 Å, which is very close to the standard value ($\alpha = 8.409$ Å) of this compound.[18]

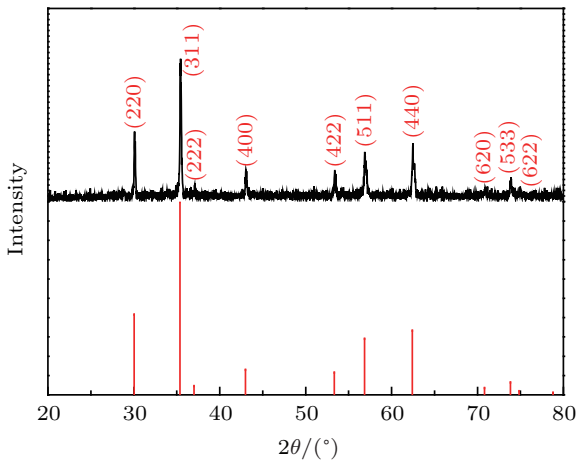


Fig. 1. (color online) The experimental XRD pattern (upper) and the standard characteristic peaks of ZnV_2O_4 (lower).

The temperature-dependent susceptibility of the sample is exhibited in Fig. 2(a). Our χ–T curve shows similar characteristics to those obtained by Vasiliev.[14] Two obvious peaks locate at $T_S = 50.1$ K and $T_M = 37.9$ K, which correspond to the structural transition and the magnetic transition, respectively. The transition temperatures are close to those obtained by Ueda and Lee from the susceptibility measurement of ZnV_2O_4, $T_S = 50$ K and $T_M = 40$ K.[7,19]

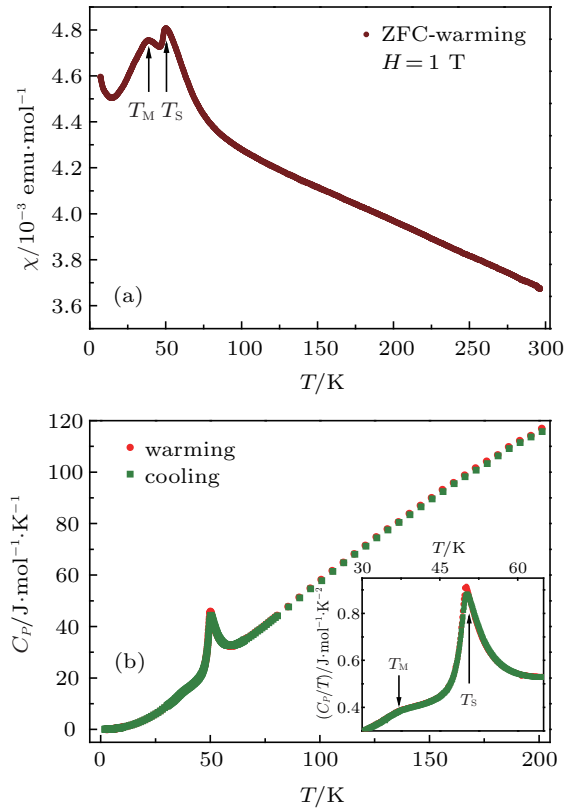


Fig. 2. (color online) (a) Temperature-dependent susceptibility of ZnV_2O_4 by ZFC-warming measurement. (b) Temperature-dependent specific heat of ZnV_2O_4 by warming (solid red dots) and cooling (solid green squares) measurement. The inset shows C_P/T vs. T for obviously displaying the peak and bump.

Figure 2(b) shows the temperature dependence of specific heat, where the solid red dots correspond to C_P measured in the cooling process, and the solid green squares represent those in the warming process. When $T < 30$ K, C_P monotonously decreases with the temperature dropping. When 30 K $\leq T \leq$ 80 K, a sharp peak around 50 K and a small bump around 35 K could be observed, corresponding to the aforementioned structural and orbital transition and magnetic transition, respectively. The peak and the bump can be more easily viewed in the C_P/T vs. T curve as displayed in the inset of Fig. 2(b). The C_P of ZnV_2O_4 in this paper is of the same order of magnitude as that obtained by Vasiliev,[14] but the transition temperatures we observed are closer to those obtained by Ueda *et al*. and Lee *et al*. through the temperature-dependent susceptibility.[7,19] Around 50 K, there is an obvious hysteresis between C_P vs. T curves obtained in cooling and warming processes, indicating that the structural transition accompanied with orbital order is a first-order transition; while at 35 K, the C_P curves are in good coincidence, implying that the antiferromagnetic transition is a second-order one. It is worth mentioning here that the deviation between cooling and warming C_P curves around 200 K may be from the thermal disturbance during the measurement process.

In the following parts, C_P will be analyzed in detail in three different temperature regions: 1) the low temperature region with $T < 30$ K, 2) the first-order structural and orbital transition region around $T_S = 50$ K, and 3) the second-order AFM transition region around $T_M = 35$ K.

3.1. Low temperature region

At low temperature, only contributions from electrons, phonons, and magnons need to be considered. Therefore, C_P can be expressed as[20]

$$C_P = \gamma T + \beta T^3 + \delta T^3, \tag{1}$$

where γ, β, and δ are electrons, phonons, and magnons coefficients, and T is the temperature. Equation (1) can be rewritten as

$$\frac{C_P}{T} = \gamma + (\beta + \delta)T^2. \tag{2}$$

According to the above equation, C_P/T should be linearly depending on T^2. Figure 3 shows C_P/T vs. T^2 in the low temperature region. As can be seen, in temperature range of 2–5 K, C_P/T–T^2 shows a good linear relationship.

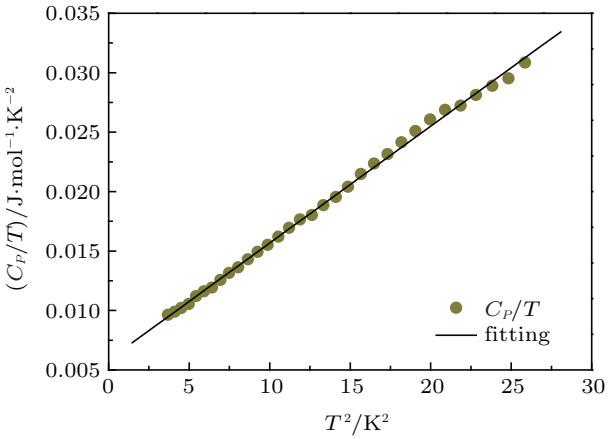


Fig. 3. (color online) Linear relationship between C_P/T and T^2 in temperature range of 2–5 K.

Through linear fitting, γ and $(\beta + \delta)$ are obtained. The fitting results are the same for both cooling and warming processes because they are identical in the considered temperature range. The related parameters obtained from fitting are $\gamma = 5.85 \times 10^{-3}$ J/mol·K^2 and $\beta' = (\beta + \delta) = 0.983 \times 10^{-3}$ J/mol·K^4. The γ of ZnV_2O_4 is lower than that of MnV_2O_4 (12×10^{-3} J/mol·K^2) reported by Myung-Whun *et al*.[21] In MnV_2O_4, not only 3d electrons of V^{3+} contribute to C_P, those of Mn^{2+} may also have significant contributions. This might be the reason for MnV_2O_4 to have larger γ compared with ZnV_2O_4. The γ can be related to Fermi energy ε_F and the density of states near the Fermi surface $D(\varepsilon_F)$ of ZnV_2O_4 as follows:[22]

$$\gamma = \frac{\pi^2(N_A \times 3)}{2\varepsilon_F} = \frac{\pi^2 k_B^2 D(\varepsilon_F)}{3}, \tag{3}$$

where N_A and k_B are the Avogadro constant and the Boltzmann constant, respectively. Based on γ obtained by fitting, ε_F and $D(\varepsilon_F)$ are derived to be 2.42 eV and 2.48 eV^{-1}, respectively. The relation between β and Debye Temperature Θ_D is given by[22]

$$\beta = \frac{12\pi^4(N_A \times 7)k_B}{5\Theta_D^3}. \quad (4)$$

Since $\beta \leq \beta' = 0.983 \times 10^{-3}$ J/mol·K^4, the low limit of ZnV_2O_4's Θ_D is estimated to be 240 K, which is deviated from 330 K obtained by Vasiliev *et al.* The reason for this difference is that Vasiliev fitted the data in a larger temperature range. According to our results, as the temperature goes up, the C_p/T vs. T^2 curve significantly deviates from a straight line.

3.2. Structural and orbital transition region

The peaks around 50 K in C_P curves for both cooling and warming processes correspond to the structural transition. Excess specific heat ΔC_P is obtained by subtracting the regular contribution from C_P and shown in Fig. 4(a). The hysteresis of ΔC_P between cooling and warming processes is more obvious here, which is strong evidence indicating that the transition here is a first-order one. The transition temperatures T_S for warming and cooling processes are 50.1 K and 50.3 K, respectively. The T_S for the warming process is exactly the same as that obtained from the temperature dependent susceptibility (shown in Fig. 2). Through the ΔC_P curve, the enthalpy change ΔH and entropy change ΔS could be calculated and the results are shown in Table 1. The Clausius–Clapayron equation on this transition could be written as[23]

$$\frac{dP}{dT} = \frac{\Delta H}{T_S(v_2 - v_1)}, \quad (5)$$

where P is the pressure, ΔH is the enthalpy change equal to the latent heat, T_S is the transition temperature, and v_1 and v_2 are the specific volumes before and after the transition, respectively. The $v_2 - v_1$ could be derived from the lattice constant and the compression ratio.[7] At T_S, the derivative of pressure with respect to temperature for temperature decreasing, $dP/dT = 9.88 \times 10^6$ Pa/K, is greater than that for temperature increasing (8.58×10^6 Pa/K).

Table 1. Enthalpy change, entropy change, and specific volume difference after and before structural transition of ZnV_2O_4 in warming and cooling measurement.

	ΔH/J·mol^{-1}	ΔS/J·mol^{-1}·K^{-1}	ΔV/m^3·mol^{-1}
Warming	115.68	2.24	2.69×10^{-7}
Cooling	−133.63	−2.55	-2.69×10^{-7}

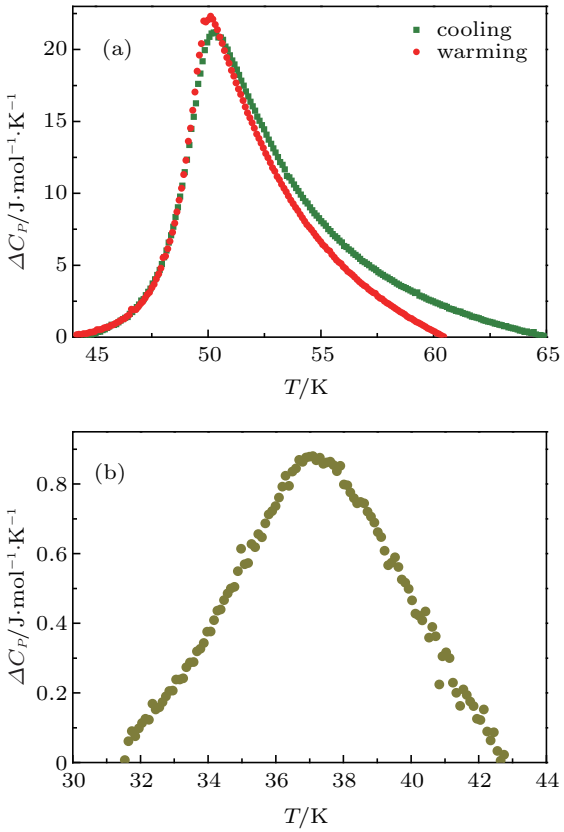


Fig. 4. (color online) (a) The excess specific heat of ZnV_2O_4 at structural transition for warming (solid red dots) and cooling (solid green squares) processes. (b) The excess specific heat of CdV_2O_4 at AFM transition for both processes.

3.3. Antiferromagnetic transition region

The bump in the C_P curve shown in Fig. 2(b) in the temperature range of 30 K to 40 K corresponds to the AFM transition of ZnV_2O_4. The coincidence of the C_P–T curves for both cooling and warming processes in this temperature range confirms that this transition is a second-order phase transition. Since the orbits have already been ordered, besides the spin–spin interaction, the spin–orbital interaction also exists, and may have a significant effect on the critical behaviors of this transition. The excess specific heat of this transition is obtained by using the same method described previously. The ΔC_P vs. T curve for the AFM transition region is shown in Fig. 4(b). The transition temperature 37.1 K is approximating to that obtained from the susceptibility measurement, 37.9 K. Theoretically, the latent heat should not exist in the second-order transition, however the excess specific heat has an apparent cusp with $\Delta C_P = 0.88$ J/mol K at $T_M = 37.1$ K. Instead of the simple step classically associated with a second-order transition, the cusp of excess specific heat signifies the contributions from thermal and spin fluctuations.[24] According to the analysis of Mozurkewich,[25] such fluctuation behavior of C_P near T_M can be divided into two regions: one is the critical region where the critical fluctuations play a crucial role, and

the other lies outside the critical region where Gaussian fluctuations are dominant. In the region of Gaussian fluctuation, the specific heat could be described as[25]

$$C_P = \sum_{n=0}^{3} a_n T^n + \frac{G}{(T - T_{\rm M})^{1/2}}, \quad T > T_{\rm M}, \tag{6a}$$

$$C_P = \sum_{n=0}^{3} a_n T^n + \frac{\sqrt{2}G}{(T - T_{\rm M})^{1/2}} + HT, \quad T < T_{\rm M}, \tag{6b}$$

where the polynomial sum represents a smooth background variation, H is the magnitude of the mean-field step, and G is the strength of the Gaussian term whose form assumes three-dimensional fluctuations. The valid area of Gaussian fluctuations is found as follows. We take a_n, G, and H as the adjustable parameters and fit the C_P curve with formulas (6a) and (6b) in the temperature region $|T - T_{\rm M}| > T^*$ by minimizing the square error σ^2. The T^* dependence of G and σ^2 is shown in Fig. 5. When $T^* \leq 0.5$ K, with the increase of T^*, σ^2 drops drastically to the minimum, while G enhances quickly; when $T^* > 0.5$ K, as T^* increases, σ^2 is almost unchanged and the enhancement of G is comparatively slow, indicating that the data no longer diverge much from the Gaussian prediction. Thus the width of the critical region of ZnV_2O_4 is $T^* = 0.5$ K. In the critical region, the critical behavior is further analyzed by renormalization-group theory, the excess specific heat could be described as[26–28]

$$\Delta C_P = A^{\pm} |t|^{-\alpha} (1 + F^{\pm} |t|^{0.5}), \tag{7}$$

where $t = (T - T_{\rm M})/T_{\rm M}$ is the reduced temperature, A^+ and A^- are the critical amplitudes of specific heat above and below the transition temperature, respectively, α is the critical exponent, and F^+ and F^- are the amplitudes of the antiferromagnetic empirical correction term. The critical exponent α depends on dimension d and order parameter n of the system.[15] Renormalization-group theory classifies such critical behavior into three different universality classes: 3D Ising model, 3D XY model, and 3D Heisenberg model.[15] By using formula (7), we fit the excess specific heat cusp in the critical region, as shown in Fig. 6. The obtained critical exponent and amplitude ratio are $\alpha = -0.011$, and $A^+/A^- = 1.46$, respectively. With these two coefficients, the specific heat curve in the critical region distributes into two separate branches above and below $T_{\rm M}$, indicating the authenticity of the critical exponent fitting. By comparing the critical exponent α and the amplitude ratio A^+/A^- with the theoretical values listed in Table 2,[29–32] we find that the amplitude ratio inclines to and slightly deviates from that of the 3D Heisenberg model, while the critical exponent α is close to that of the 3D XY model.

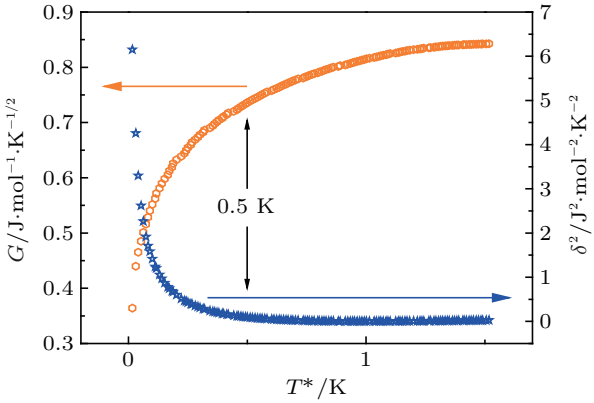


Fig. 5. (color online) The T^* -dependent strength of the Gaussian term G (hollow orange hexagons) and square error σ^2 (hollow blue stars).

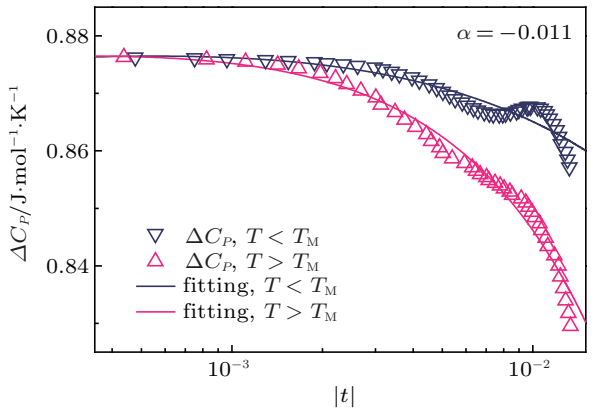


Fig. 6. (color online) Experimental (triangles) and fitted curves (lines) of the specific heat vs. reduced temperature above (pink) and below (navy blue) $T_{\rm M}$ for PM–AFM transition of ZnV_2O_4.

Table 2. Critical exponents and critical amplitude of ZnV_2O_4; theoretical values of different models.

Model	Critical exponent α	Critical amplitude ratio A^+/A^-
3D Ising	0.11	0.52
3D XY	−0.014	1.06
3D Heisenberg	−0.115	1.52
This work	−0.011	1.46

To understand the abnormal critical behaviors of ZnV_2O_4, it is helpful to compare the critical behaviors of ZnV_2O_4 with those of MnV_2O_4, since they are isostructural counterparts. In MnV_2O_4, the second-order transition is ferrimagnetic and happens at higher temperature than the structural and orbital transition. So for MnV_2O_4, around $T_{\rm M}$, the orbital order is lacking, and the spin–spin interactions dominate this second-order transition. Nevertheless, the investigation of DC-magnetization by Zhang's group revealed that magnetic critical exponent β deviates from the 3D Heisenberg model and proposed that the deviation is due to the precursor phenomenon of orbital order fluctuation.[16] For ZnV_2O_4, $T_{\rm M} < T_{\rm S}$, i.e., around $T_{\rm M}$ of ZnV_2O_4, the orbital order has already presented. So the spin–spin and spin–orbital interactions

coexist at T_M and both of them contribute to the transition. Therefore, strong spin–orbital coupling might confine the spin degree of freedom, and also induces the universality class of critical behaviors to deviate from the 3D Heisenburg model, even shifting to the 3D XY model.

4. Summary

The phase transition and low temperature characteristics of spin–orbital coupling spinel ZnV_2O_4 are investigated. The Debye temperature, the Fermi energy, and the density of states near the Fermi surface of this compound are given by analyzing the data of specific heat below 5 K. The measurement of temperature-dependent specific heat confirms that the structural transition accompanied with orbital order at $T_S = 50.1$ K is a first-order one, while the AFM transition at $T_M = 37.1$ K is a second-order phase transition. For the first-order structural and orbital transition, the enthalpy and entropy change are calculated, meanwhile, the derivative of pressure with respect to temperature $\mathrm{d}P/\mathrm{d}T$ at T_S is estimated by using the Clausius–Clapayron equation. For the second-order AFM transition, the analysis of the critical behavior estimates the width of the critical fluctuation region to be about 0.5 K, and also finds that the critical amplitude ratio deviates from the theoretical value of the 3D Heisenberg model, while the critical exponent α is close to that of 3D XY model. This kind of abnormal critical behavior might be attributed to the influences of spin–orbital coupling.

References

[1] Butt F K, Cao C, Ahmed R, Khan W S, Cao T, Bidin N, Li P, Wan Q, Qu X, Tahir M and Idrees F 2014 *Cryst. Eng. Comm.* **16** 894

[2] Butt F K, Tahir M, Cao C, Idrees F, Ahmed R, Khan W S, Ali Z, Mahmood N, Tanveer M, Mahmood A and Aslam I 2014 *ACS Appl. Mater. Inter.* **6** 13635

[3] Xiao L, Zhao Y, Yin J and Zhang L 2009 *Chemistry* **15** 9442

[4] Butt F K, Cao C, Wan Q, Li P, Idrees F, Tahir M, Khan W S, Ali Z, Zapata M J M, Safdar M and Qu X 2014 *Int. J. Hydrogen. Energ.* **39** 7842

[5] Anderson P W 1956 *Phys. Rev.* **102** 1008

[6] Reehuis M, Krimmel A, Büttgen N, Loidl A and Prokofiev A 2003 *Eur. Phys. J. B* **35** 311

[7] Ueda Y, Fujiwara N and Yasuoka H 1997 *J. Phys. Soc. Jpn.* **66** 778

[8] Maitra T and Valentí R 2007 *Phys. Rev. Lett.* **99** 126401

[9] Tsunetsugu H and Motome Y 2003 *Phys. Rev. B* **68** 060405(R)

[10] Motome Y and Tsunetsugu H 2005 *Prog. Theor. Phys. Suppl.* **160** 203

[11] Tchernyshyov O 2004 *Phys. Rev. Lett.* **93** 157206

[12] Nizioł S 1973 *Phys. Stat. Sol. A* **18** K11

[13] Izyumov Yu A, Naish V E and Petrov S B 1979 *J. Magn. Magn. Mater.* **13** 267

[14] Vasiliev A N, Markina M M, Isobe M and Ueda Y 2006 *J. Magn. Magn. Mater.* **300** e375-

[15] Feng D, Jin G J 2013 *Condensed Matter Physics* (Volume II) (Beijing: Higher Education Press) (in Chinese) pp. 32–36, 66–69

[16] Zhang L, Han H, Qu Z, Fan J, Ling L, Zhang C, Pi L and Zhang Y 2014 *J. Appl. Phys.* **115** 233910

[17] Luo X, Yang Z R, Sun Y P, Zhu X B, Song W H and Dai J M 2009 *J. Appl. Phys.* **106** 113920

[18] Ebbinghaus S G, Hanss J, Klemm M and Horn S 2004 *J. Alloys Compd.* **370** 75

[19] Lee S H, Louca D, Ueda H, Park S, Sato T, Isobe M, Ueda Y, Rosenkranz S, Zschack P, Íñiguez J, Qiu Y and Osborn R 2004 *Phys. Rev. Lett.* **93** 156407

[20] Tari A 2003 *The Specific Heat of Matter at Low Temperatures* (London: Imperial College Press) pp. 33, 66, 152–153

[21] Myung-Whun K, Kim J S, Katsufuji T and Kremer R K 2011 *Phys. Rev. B* **83** 024403

[22] Lu D , Jiang P and Xu Z Z 2003 *Solid State Physics* (Shanghai: Shanghai Science and Technology Press) (in Chinese) pp. 113, 79

[23] Fujimoto M 2005 *The Physics of Structural Phase Transitions* (Berlin: Springer-Verlag) p. 7

[24] Chandra P 1989 *J. Phys: Condens. Matter* **1** 10067

[25] Mozurkewich G 1991 *Phys. Rev. Lett.* **66** 1645

[26] Gamzatov A G, Khizriev K S, Batdalov A B, Abdulvagidov S B, Aliev A M, Melnikov O V and Gorbenko O Y 2009 *Low Temp. Phys.* **35** 214

[27] Gamzatov A G, Aliev A M, Khizriev K S, Abdulvagidov S B, Batdalov A B, Gorbenko O Y and Melnikov O V 2007 *Physica B* **390** 155

[28] Gamzatov A G, Aliev A M, Khizriev K S, Kamilov I K and Mankevich A S 2011 *J. Alloys Compd.* **509** 8295

[29] Guida R and Zinn-Justin J 1998 *J. Phys. A: Math. Gen.* **31** 8103

[30] Campostrini M, Hasenbusch M, Pelisseto A, Rossi P and Vicari E 2001 *Phys. Rev. B* **63** 214503

[31] Campostrini M, Hasenbusch M, Pelisseto A, Rossi P and Vicari E 2002 *Phys. Rev. B* **65** 144520

[32] Oleaga A, Salazar A, Thamizhavel A and Dhar S K 2014 *J. Alloys Compd.* **617** 534